frontiers in Astronomy and Space Sciences

ORIGINAL RESEARCH
published: 30 April 2021
doi: 10.3389/fspas.2021.646895

KORTES Mission for Solar Activity Monitoring Onboard International Space Station

Alexey Kirichenko[1], Sergey Kuzin[1], Sergey Shestov[1,2], Artem Ulyanov[1], Andrey Pertsov[1], Sergey Bogachev[1], Anton Reva[1], Ivan Loboda[1], Eugene Vishnyakov[1], Sergey Dyatkov[1], Nataliya Erkhova[1], Marek Stęślicki[3], Janusz Sylwester[3], Stefan Płocieniak[3], Piotr Podgórski[3], Mirosław Kowaliński[3], Jarosław Bakała[3], Żaneta Szaforz[3], Marek Siarkowski[3], Daniel Ścisłowski[3], Tomasz Mrozek[3], Barbara Sylwester[3], Ilya Malyshev[4], Alexey Pestov[4], Vladimir Polkovnikov[4], Mikhail Toropov[4], Nikolay Salashchenko[4], Nikolay Tsybin[4] and Nikolay Chkhalo[4]*

[1] Laboratory of X-Ray Astronomy of the Sun, Optics Department, P.N. Lebedev Physical Institute of the Russian Academy of Sciences, Moscow, Russia, [2] Solar-Terrestrial Centre of Excellence—SIDC, Royal Observatory of Belgium, Brussels, Belgium, [3] Space Research Center, Polish Academy of Sciences, Warsaw, Poland, [4] Institute for Physics of Microstructures, Russian Academy of Sciences, Nizhny Novgorod, Russia

OPEN ACCESS

Edited by:
Simon Pete Worden, Independent Researcher, Menlo Park, United States

Reviewed by:
Lucia Kleint, Université de Genève, Switzerland
James Paul Mason, University of Colorado Boulder, United States

***Correspondence:**
Artem Ulyanov
ulyanovas@lebedev.ru

Specialty section:
This article was submitted to Astronomical Instrumentation, a section of the journal Frontiers in Astronomy and Space Sciences

Received: 28 December 2020
Accepted: 06 April 2021
Published: 30 April 2021

Citation:
Kirichenko A, Kuzin S, Shestov S, Ulyanov A, Pertsov A, Bogachev S, Reva A, Loboda I, Vishnyakov E, Dyatkov S, Erkhova N, Stęślicki M, Sylwester J, Płocieniak S, Podgórski P, Kowaliński M, Bakała J, Szaforz Ż, Siarkowski M, Ścisłowski D, Mrozek T, Sylwester B, Malyshev I, Pestov A, Polkovnikov V, Toropov M, Salashchenko N, Tsybin N and Chkhalo N (2021) KORTES Mission for Solar Activity Monitoring Onboard International Space Station. Front. Astron. Space Sci. 8:646895. doi: 10.3389/fspas.2021.646895

We present a description of the recent advances in the development of the KORTES assembly—the first solar oriented mission designed for the Russian segment of the International Space Station. KORTES consists of several imaging and spectroscopic instruments collectively covering a wide spectral range extending from extreme ultraviolet (EUV) wavelengths to X-rays. The EUV telescopes inside KORTES will trace the origin and dynamics of various solar phenomena, e.g., flares, CMEs, eruptions etc. EUV spectra provided by grazing-incidence spectroheliographs will enable precise DEM-diagnostics during these events. The monochromatic X-ray imager will observe the formation of hot plasma in active regions and outside them. The SolpeX module inside KORTES will offer an opportunity to measure fluxes, Doppler shifts and polarization of soft X-ray emission both in lines and continuum. SolpeX observations will contribute to studies of particle beams and chromospheric evaporation. The instrumentation of KORTES will employ a variety of novel multilayer and crystal optics. The deployment of KORTES is planned for 2024.

Keywords: solar corona, solar flares, polarimetry, spectroscopy, solar imaging, extreme ultraviolet, soft X-rays, international space station

1. INTRODUCTION

The KOronal X-Ray TElescope and Spectrometer (KORTES) is the first solar mission designed for the Russian segment of the International Space Station (ISS). The Principal Investigator (PI) of the project responsible for the majority of instrumentation is the Laboratory of X-Ray Astronomy of the Sun (XRAS) at P.N. Lebedev Physical Institute of the Russian Academy of Sciences (LPI RAS). The main collaboration members are Institute for Physics of Microstructures of the Russian Academy of Sciences (IPM RAS) from Nizhny Novgorod, Russia, and Space Research Center of the Polish Academy of Sciences (SRC PAS) from Wroclaw, Poland. The project successfully passed the stages from initial proposal to engineering design; its development is currently on the stage of certification and qualification tests and the launch is planned on 2024.

KORTES is a conceptual successor of the previous XRAS projects—SPIRIT (SPectrohelIogRaphIc Telescope) and TESIS (TelEScope and Imaging Spectrometer) launched within the Russian CORONAS program (Complex ORbital Observations of Near-Earth Activity of the Sun). Similar to these projects KORTES represents a multichannel assembly of telescopes and spectrometers to cover a wide range of wavelengths—from hard X-rays (0.44 Å) to extreme ultraviolet (584 Å). KORTES inherits optical design of some instruments from its predecessors (Shestov S. V. et al., 2014). Apart from that, several new technologies will be probed, e.g., novel aperiodic multilayer structures (Akhsakhalyan et al., 2019) and fine stabilization system. A successful appliance of these technologies will advance their adoption in the future projects of XRAS, such as ARKA—a challenging new experiment for high-resolution imaging of solar corona (Vishnyakov et al., 2017).

The main technical parameters of KORTES are listed in **Table 1**. Stationing on-board ISS has several advantages with respect to telemetry rate (which is almost limitless considering the possibility of data storage on removable flash cards) and limits on mass and size of the payload. However, due to obstruction by the elements of ISS construction the nominal duty cycle of KORTES is reduced to 25 min per orbit (or 6.5 h per day).

TABLE 1 | Main technical parameters of KORTES.

Mass	48.9 kg (SU), 10 kg (EU)
Dimensions, $L \times W \times H$	89 × 49 × 44 cm (SU), 25 × 20 × 10 cm (EU)
Power consumption	80 W (SU), 30 W (EU)
Duty cycle	6.5 hours per day
Data rate	50 MB/s
Telemetry rate	1 GB per day
Accuracy of pointing	10″ (DPP), 1″ (APS)

Also, the considerable jitter of ISS (Brown, 2019) introduces notable restrictions in terms of achievable resolution, both spatial ($>$ 4″) and temporal ($>$ 2 s). Due to that, KORTES is mainly intended to meet goals of solar activity monitoring and space weather forecasting. Nevertheless, the KORTES facilities will also address a wide spectrum of fundamental problems in domains of solar physics and solar-terrestrial interactions (Slemzin et al., 2016, 2019; Rodkin et al., 2018; Shugay et al., 2018). KORTES will allow to study the mechanisms of solar flare generation and the formation of high-temperature plasma in active regions (ARs) and outside them, investigate statistical properties for microevents, trace the initiation and propagation of solar eruptive phenomena (prominences, coronal mass ejections) at heights up to two solar radii (Zhang et al., 2001; Byrne et al., 2014; Reva et al., 2016a,b).

KORTES consists of two separate units. The KORTES Sensors Unit (KORTES-SU) will hold the instrumentation assembly and will be placed on the multipurpose working place #4 on the service module of the ISS Russian segment. The general view of the KORTES-SU unit is presented on **Figure 1**. Since ISS has a nadir orientation KORTES-SU will be mounted on a special Dual-axis Pointing Platform (DPP) to enable coarse pointing to the Sun. DPP will partially solve the problem of the ISS jitter. Additional stabilization will be provided by instruments' internal stabilization systems. The second unit—KORTES-EU (Electronics Unit)—represents a controller aimed to drive the operation of KORTES-SU and gather, compress, and transfer scientific data. The most part of image processing will be produced on ground (Kuzin et al., 2011a). KORTES-EU will be placed inside the sealed compartment of the ISS Russian segment. The view of the KORTES-EU unit is embedded in **Figure 1** (top-right corner).

The scientific instrumentation of KORTES-SU consists of three EUV telescopes, two X-ray imagers and four spectrometers.

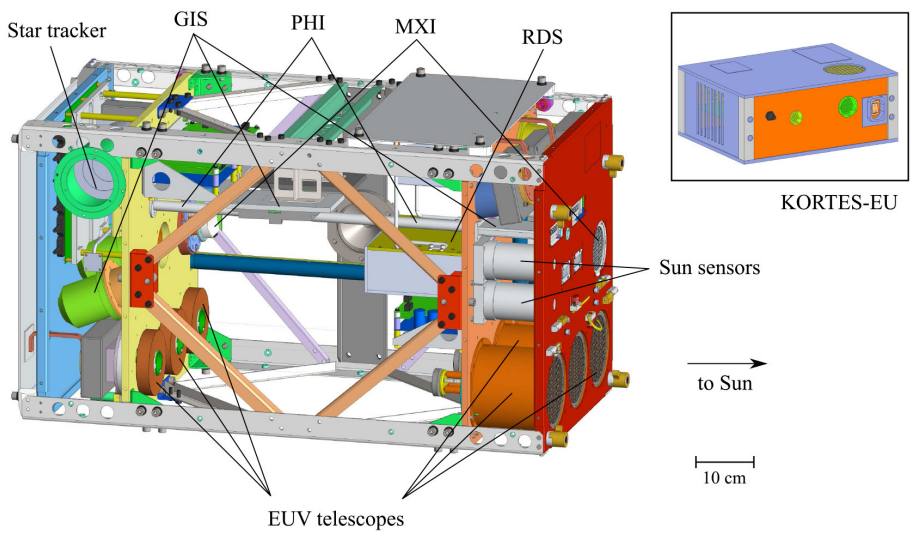

FIGURE 1 | A general view of the KORTES-SU assembly. The SU unit is to be mounted on a dual-axis pointing platform on the service module of the ISS Russian segment. Top-right corner: the KORTES-EU unit (proportions are preserved). The EU unit will be placed inside the sealed compartment of the ISS Russian segment.

TABLE 2 | Main characteristics of telescopes.

Target lines (channel)	Fe XII 195 Å (T1), He II 304 Å (T2), He I 584 Å (T3)
Entrance filters	3 layers, $MoSi_2$ (2.5 nm)/Al (235 nm)/ $MoSi_2$ (2.5 nm)
Mirror coatings (channel)	Multilayer, Be (6 nm)/Al (10 nm) (T1, T2), Al (30 nm)/Mo (10 nm) + $MoSi_2$ (5 nm) layer (T3)
Detector coatings	3 layers, $MoSi_2$ (25 nm)/Al (235 nm)/ $MoSi_2$ (25 nm)
Primary mirror diameter	113 mm
Secondary mirror diameter	45 mm
Effective focal length	1740 mm
Detector type	CCD (e2v 42-40, BSI, TEC-cooled)
Detector size	2,048×2,048
Pixel size	13.5 μm
Angular resolution	3.2″
Field of view	$\sim 0.91^\circ$
Frame rate	1–20 fps
Exposure time	0.1–5 s
APS system	optical, 3-axis (pitch, yaw, focus)

XRAS is responsible for the majority of instrumentation (the EUV telescopes, the grazing-incidence spectroheliographs, and the monochromatic X-ray imager). The rest three instruments (the rotating drum spectrometer, the X-ray pinhole camera, and the Bragg polarimeter) are combined in a separate structural unit inside KORTES-SU called SolpeX which is being developed by SRC PAS. The details on the SolpeX module can be found in Stęślicki et al. (2016) and Sylwester et al. (2019).

In addition to the scientific instruments KORTES-SU includes three guidance sensors (two Sun sensors and a star tracker) aimed to support accurate pointing and facilitate stabilization. The mechanical design of KORTES-SU is of modular type with all instruments being installed on a single invar frame to sustain temperature variations of up to $\pm 25^\circ$C. Additionally, the thermal regime of KORTES-SU is balanced with a radiator mounted on the backside of the unit. The electrical communication between the devices and the controller is provided by a hub connected to KORTES-EU via the Hotlink interface.

In the following the design of the separate KORTES instruments is described in more details.

2. EUV TELESCOPES

The EUV imaging subsystem of KORTES consists of three similar Ritchey-Chretien telescopes with multilayer normal-incidence optics adapted to different wavelengths, referred to as T1, T2, and T3 spectral channels (see **Table 2**). The T1 channel is centered at 195 Å line of Fe XII ion and is dedicated to image coronal plasma with temperature near 1 MK. The T2 channel corresponds to famous He II 304 Å line and aims at transition region ($T \approx 80,000$ K). The T3 channel specializes at upper chromosphere layer (He I 584 Å line, $T \approx 20,000$ K).

The telescopes share the same optical scheme and consist of an entrance aperture assembly, two mirrors (primary and secondary), a mechanical shutter and a CCD detector (see **Figure 2**). The effective focal length of all three telescopes equals to 1,740 mm giving a field of view (FoV) of 0.91° to enable wide-field observations of CME formation and flux-rope eruptions. The main advantage of the KORTES telescopes over other EUV telescopes and coronographs, e.g., LASCO/C2 and C3 (Brueckner et al., 1995) or SDO/AIA (Lemen et al., 2012), is that they may provide valuable observations in the so-called "blind zone"—the gap in solar altitudes between 1.2 and 2 solar radii (Reva et al., 2014, 2017).

The aperture of the telescopes' primary mirrors equals to 113 mm. The secondary mirrors have a diameter of 45 mm. The images are obtained with 2 ×2 k backside-illuminated (BSI) e2v 42-40 CCDs cooled by a Peltier thermoelectric coolers (TEC). The aberrations of the optical scheme (mostly dominated by astigmatism and field curvature) were optimized so that the circle of confusion is contained within one pixel of a CCD (13.5 ×13.5 μm) over the entire FoV, which ensures angular resolution (double pixel angular size) of 3.2″.

The mounts of the secondary mirrors are equipped with an active positioning system (APS) to enable fine pointing and stabilization which operates alongside with the DPP system. The pointing correction signal is feeded by two Sun sensors mounted at the front of KORTES-SU. The APS unit includes three piezoelectric actuators, capable of pitch and yaw adjustments in a range of $\pm 15'$, and a linear stepping motor with a range of up to ± 50 μm. The latter is used to compensate for possible defocusing resulting from the thermal expansion of the KORTES-SU supporting frame.

The multilayer structures for the KORTES telescopes are developed in IPM RAS (Bogachev et al., 2016; Vishnyakov et al., 2016). The parasite optical and infrared radiation is blocked by a $MoSi_2$/Al entrance filter (Chkhalo et al., 2018) and CCD coating ($MoSi_2$/Al as well). These are identical for all telescopes. The individual spectral band for each telescope is determined by the convolution of spectral reflectivities of the primary and secondary mirrors. The mirror coatings are based on the multilayer Be/Al (for the T1 and T2 channels) and Al/Mo (T3) structure. The mirror reflectivity peaks at 35% for the 195 and 584 telescopes and 25% for the 304 telescope resulting in effective areas of around 0.5–4 cm^2 (depending on the channel).

The exposure and cadence of telescopes will be dynamically adjusted with respect to the current state of the solar activity, defined with the PHI instrument. The typical values of exposure are expected to range from 0.1 to 5 s. The maximum cadence of $\sim$ 1 full resolution image per second is limited by data transfer speed of the Hotlink interface connecting KORTES-SU and KORTES-EU (50 MB/s). However, the KORTES telescopes will be able to achieve even higher cadence (up to 20 frames per second) in a high-speed mode of operation with a partial frame readout. KORTES will automatically switch to this mode during the impulsive phase of flares. Additionally, special high-cadence series of observations will be carried out to study high-speed solar phenomena, e.g., nanoflares (Ulyanov et al., 2010, 2019a,b), waves (Shestov et al., 2015, 2017), and transients (Loboda and Bogachev, 2015a,b, 2017, 2019).

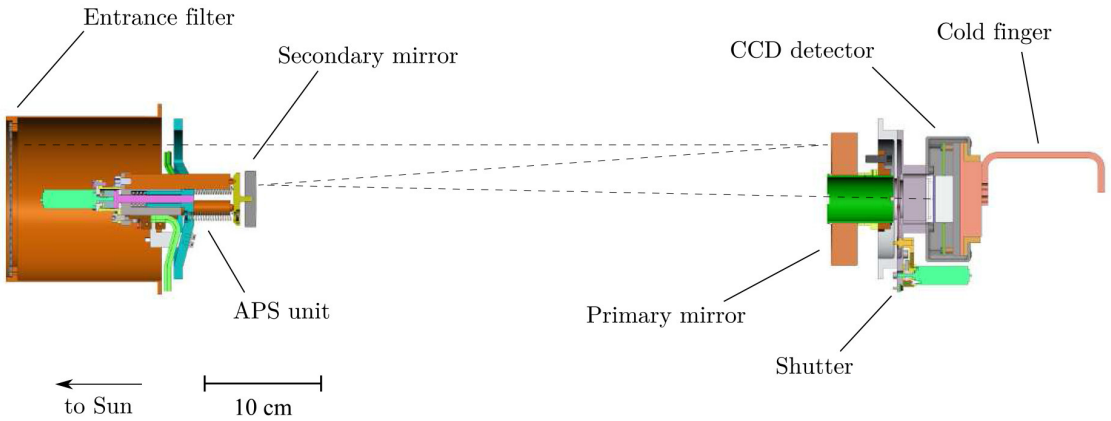

FIGURE 2 | A cross sectional view of the EUV telescopes inside the KORTES-SU assembly. The three KORTES telescopes share the same Ritchey-Chretien optical design with 113 mm aperture and 1,740 mm effective focal length. The secondary mirrors feature an active positioning system (APS) to enable fine pointing and stabilization.

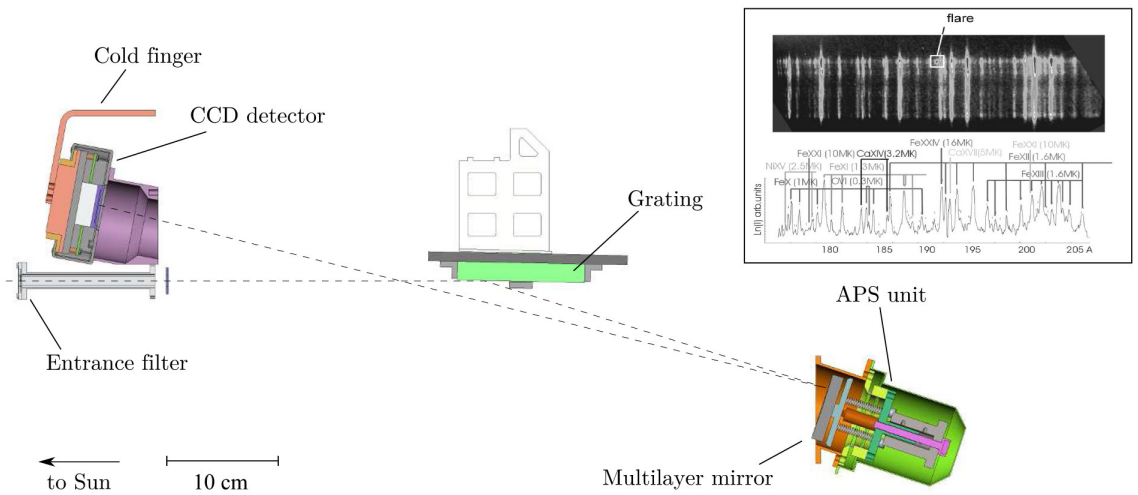

FIGURE 3 | A cross sectional view of the Grazing-Incidence Spectroheliographs (GIS) inside the KORTES-SU assembly. Top-right corner: an example of a solar spectrum (obtained with the SPIRIT instrument on 25 September, 2001). Each "cigar" on the top represent a monochromatic image of the Sun squeezed in the direction of dispersion. The corresponding spectral lines are shown at the bottom.

3. GRAZING-INCIDENCE SPECTROHELIOGRAPHS

The KORTES EUV Grazing-Incidence Spectroheliographs (GIS) incorporate a unique slitless optical design inherited from previous XRAS missions TESIS (Zhitnik et al., 2002) and SPIRIT (Kuzin et al., 2011b). The key element of these instruments is a flat gold-coated reflecting grating. The radiation diffracted from the gratings is then focused by a normal-incidence multilayer mirrors onto CCD detectors (see **Figure 3**). KORTES will have two GIS instruments on-board, which are designated as S1 and S2. The S1 channel is designed to cover the spectral range from 170 to 190 Å, while the S2 channel embraces the wavelengths from 280 to 335 Å. In both channels the gratings' groove density equals to 1,200 lines per mm. The chosen diffraction order is $m = 3$. The focusing mirrors are off-axis paraboloid with $F = 703$ mm effective focal distance and $D = 58$ mm aperture. The detectors are cooled e2v 42-40 2 ×2 k CCDs and provide wide FoV of more than 2°. The main parameters of the two spectroheliographs are listed in **Table 3**.

The significant difference between incidence and diffraction angles results in a pronounced anamorphic magnification (Schweizer, 1979), so that the images of the Sun in separate spectral lines become squeezed by a factor of ≈ 20. As the spectroheliographs' linear dispersion is ≈ 0.6 mm/Å, the "cigars" from the neighboring spectral lines are weakly blended and can be easily separated. The rough appearance of an overall solar "cigarogram" can be traced from images obtained with SPIRIT

GIS (see example on **Figure 3**), top-right corner. Though large portion of spatial information is wasted, the position of small compact sources on the disk (e.g., flares) can be located with enough precision. The topology of these sources will be refined with telescopic data. Another type of objects of interest to be observed is structures located high above the limb (e.g., CMEs).

TABLE 3 | Main characteristics of grazing-incidence spectroheliographs (GIS).

Spectral range (channel)	170–190 Å (S1), 280–335 Å (S2)
Target ions (channel)	Fe X–Fe XIII, Ca XVII (S1), Fe XIII–Fe XVII, Ca XVIII, Si IX, Si XI, Ni XVIII, S XII, Mg XIII (S2)
Entrance filters	3 layers, $MoSi_2$ (2.5 nm)/Al (235 nm)/$MoSi_2$ (2.5 nm)
Mirror coatings (channel)	Multilayer, Mo/Si (220 nm)
Detector coatings	3 layers, $MoSi_2$ (25 nm)/Al (235 nm)/$MoSi_2$ (25 nm)
Mirror diameter	58 mm
Effective focal length	703 mm
Detector type	CCD (e2v 42-40, BSI, TEC-cooled)
Detector size	2,048×2,048
Pixel size	13.5 μm
Angular resolution	7.9″
Field of view	∼ 2.2°
Grating groove density	1,200 lines per mm
Linear dispersion	0.6 mm/Å
Grating blaze angle (channel)	9.0° (S1), 11.5° (S2)
Incidence angle (channel)	1.16° (S1), 1.40° (S2)
Diffraction angle (channel)	21.35° (S1), 27.38° (S2)
Exposure time	10–30 s
APS system	hybrid, 2-axis: optical (spatial axis), electronic (spectral axis)

The working spectral range of the KORTES "cigarographs" is mainly defined by spectral reflectance of mirrors' multilayer structures. KORTES GISes will feature novel optimized aperiodic Mo/Si structures designed in IPM RAS (Garakhin et al., 2020; Kuzin et al., 2020). The passband of the S1 channel will cover strong lines of ions Fe X–Fe XIII and Ca XVII. The second channel (S2) will register, apart from He II 304 Å line, the lines of Fe XIII–Fe XVII, Ca XVIII, Si IX, Si XI, Ni XVIII, S XII, and Mg XIII (Shestov S. et al., 2014). Many of these lines are blended and hence some advanced techniques for DEM reconstruction should be implemented to extract physical parameters from observables (Shestov et al., 2009).

An estimated exposure time amounts to 10–30 s. In order to avoid motion blur the spectroheliographs will be equipped with a stabilization system as well. However, due to anamorphic magnification the stability requirements along the direction of dispersion are reduced. Hence the mechanical stabilization (by means of mirror tilting) will operate along a single (spatial) axis. Nevertheless, the second (spectral) axis will be stabilized electronically–via CCD charge transfer.

4. MONOCHROMATIC X-RAY IMAGER

The monochromatic X-ray Bragg-crystal Imager (MXI) is a simple, yet a very powerful device. The instruments of this type proved their effectiveness for hot plasma imaging in the previous XRAS missions (Zhitnik et al., 2003; Bogachev et al., 2020). MXI is aimed to image the Sun in a single line of hydrogen-like Mg XII–Ly$_\alpha$ 8.42 Å. The optical layout of Mg-imager consists of an entrance window, an off-axis mirror and an image detector (see **Figure 4**). The mirror is made of quartz plate bent to a spherical shape with a curvature radius of $R = 1,176$ mm. The lattice plane [010] of quartz with $2d \approx 8.51$ Å is utilized. The detector is 1k×1k BSI CCD-matrix with a frame transfer feature

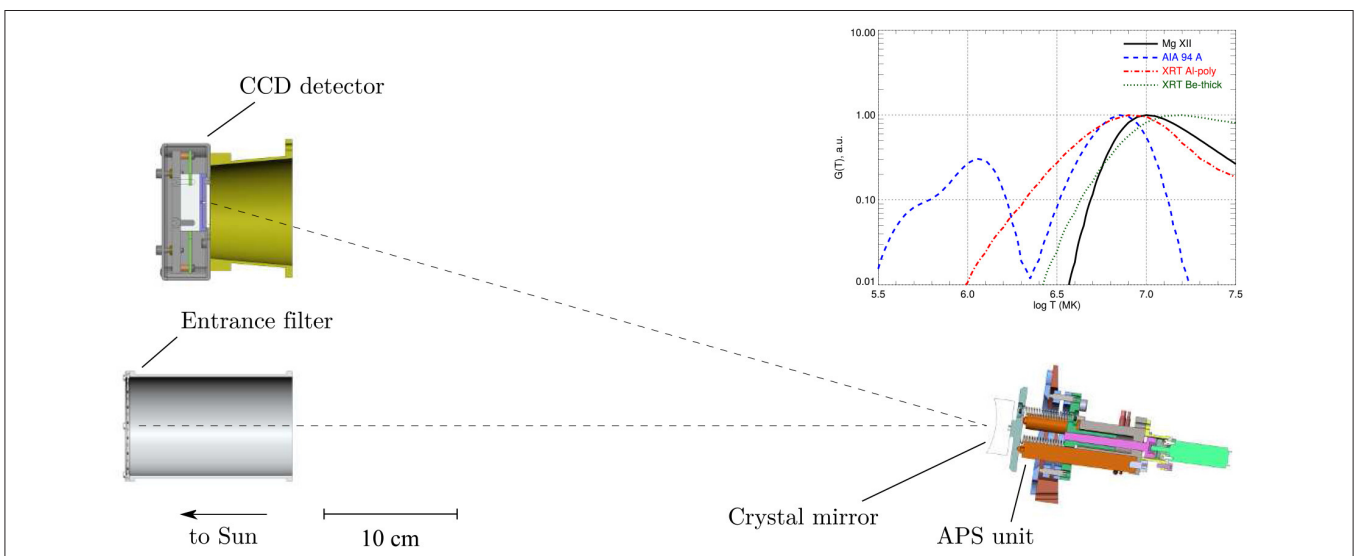

FIGURE 4 | A cross sectional view of the Monochromatic X-ray Imager (MXI) inside the KORTES-SU assembly. Top-right corner: the temperature response function of MXI in comparison with SDO/AIA and Hinode/XRT. MXI is sensitive only to "hot" (T>4 MK) plasma component in contrast to other imagers.

TABLE 4 | Main characteristics of monochromatic X-ray Bragg-crystal imager (MXI).

Target line	Mg XII Ly$_\alpha$ 8.42 Å
Entrance filter	3 layers, $MoSi_2$ (2.5 nm)/Al (235 nm)/$MoSi_2$ (2.5 nm)
Detector coating	3 layers, $MoSi_2$ (25 nm)/Al (235 nm)/$MoSi_2$ (25 nm)
Mirror	Bent quartz (spherical), [010] lattice plane, $2d \approx 8.51$ Å
Mirror dimensions	60 ×40 mm
Mirror radius	1,176 mm
Effective focal length	582 mm
Detector type	CCD (e2v 47-20, BSI, frame transfer, TEC-cooled)
Detector size	1,024×1,024
Pixel size	13 μm
Angular resolution	9.2″
Field of view	$\sim 1.3^\circ$
Exposure time	10–100 s
APS system	optical, 3-axis (pitch, yaw, focus)

(e2v 47-20). MXI will also be equipped with an APS system (same as in telescopes). The main parameters of the MXI instrument are listed in **Table 4**.

Despite relatively large area of the mirror (60 ×40 mm), its effective aperture is narrow because incident rays reflect only from those parts of it where the Bragg condition is satisfied. Hence the effective aperture of the mirror is defined only by its length. The second dimension is a trade-off between two requirements: it should be quite narrow to reject the neighboring spectral lines, but wide enough to cover the whole area of the detector. With the given width the bandpass of the mirror amounts to $\Delta\lambda \approx 0.015$ Å, while the nearest line (Na XI 8.454 Å) is 0.03 Å apart from the target line.

The target spectral line of Mg XII is forming under temperatures above 4 MK. As soon as no other strong lines fall into the bandpass of the mirror, the device will be totally insensitive to emission of "cold" ($T < 0.5$ MK) and "warm" ($T \approx 1$ MK) plasma. Hence the MXI images are free from unwanted low-temperature background usually present on images of analogous telescopes (e.g., SDO/AIA, Hidone/XRT, RHESSI). This feature makes MXI an ideal choice to observe plasma at temperatures above 4 MK (Reva et al., 2012, 2015, 2018; Kirichenko and Bogachev, 2013, 2017a,b).

It should be noted, that Mg XII line represents a doublet with a wavelength offset of around 5 mÅ. In theory, due to spherical aberration existing in the system, the device should resolve both components of the doublet leading to noticable splitting of the image in the dispersion direction. However, as the ratio of component intensities is established (Sylwester et al., 1986), this unwanted effect can be easily corrected via computational techniques (e.g., by image deconvolution).

5. ROTATING DRUM SPECTROMETER

The Rotating Drum X-ray spectrometer (RDS) is a part of the SolpeX module inside the KORTES-SU unit. RDS will allow to investigate very fast changes in X-ray solar spectra occurring during the impulsive phase of flares. The RDS consists of eight flat mono-crystals attached to a rotating drum (see **Figure 5**). The drum rotation speed is fixed at 10 turns per second and defines the cadence of measurements. At a given instant of time four of the crystals are illuminated by the solar radiation coming through a pair of entrance apertures covered by aluminum-coated Lexan foil filters to block thermal, optical and EUV radiation. The Bragg-reflected photons are recorded by two pairs of Silicon Drift Detectors (SDD) placed symmetrically. Under full drum revolution each of the crystals passes all of the detectors. The rotation of the drum allow to scan the spectra of the radiation reflected from the crystals at slightly different Bragg angles. Moreover, as each crystal appears to incline at different angles with respect to front and rear detectors it covers two spectral wavebands. As a result a wide continuous range from 0.4 to 22.8 Å is covered merely in 0.1 s. This procedure will allow to determine spectral line fluxes for many abundant elements (from oxygen to iron) emitted from flaring plasma with temperatures between 1 and 50 MK.

The parameters of crystals and the corresponding energy ranges are presented in **Table 5**. Two out of eight RDS crystals are identical Si 111. Their position on the drum is such that they can simultaneously illuminate a pair of rear detectors. This enables a Dopplerometer functionality of RDS.

The Bragg-angle (and hence energy) of reflected photons is estimated from the photon arrival time and the corresponding drum position. With utilized KETEK VITUS H18LE and H50 SDD detectors and supplemented electronics the detection time will be established with accuracy of $\sim 1\mu$s. This uncertainty defines the spectral resolution of the instrument. The SDDs will be cooled down to -20°C with the built-in TECs. The detector temperatures will be monitored by the thermistor and controlled by the FPGA logic.

The rotating drum is actuated by a stepper motor operating in a microstepping mode with 6,400 microsteps per revolution. The position of the drum is measured by a magnetic sensor with a resolution of 12 bits per revolution. An overall accuracy accounting for time and angle errors is estimated to be better than 20 arcsec.

6. PINHOLE SOFT X-RAY IMAGER

Since RDS does not provide any spatial information an imaging device of the similar spectral range is required to co-align the sources of X-ray spectra with active regions seen on the telescopic images. Such information can be obtained from a simple PinHole Imager (PHI). The optical layout of this instrument consists of an entrance filter to reject thermal/optical/EUV radiation, a lead foil with a pin hole and an image sensor (see **Figure 6**). A filter is made of 15μm-thick aluminized polyimide foil and will transmit in the range $E > 0.35$ keV (similar to Hinode XRT Ti-poly filter). The sensor is 2 ×2 k CMOS made by Gpixel Inc. The thickness of a lead foil is 0.4 mm, the size of a pin hole is 0.7 mm, the distance between a lead foil and a sensor—703 mm. With these dimensions the diameter of the projected solar disk equals to 595 pixels. Hence the position of the disk can be used

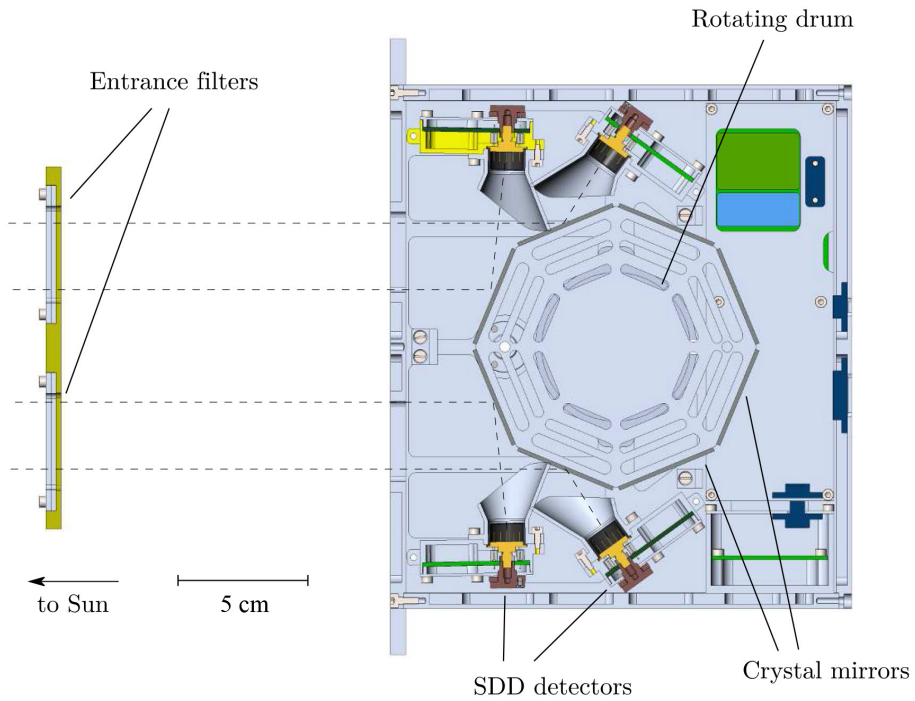

FIGURE 5 | A cross sectional view of the Rotating-Drum Spectrometer (RDS) inside the KORTES-SU assembly. The drum with eight crystals is rotating at 10 turns per second. The solar radiation reflected from the crystals is registered by four SDD-detectors placed symmetrically in a Dopplerometer configuration.

TABLE 5 | Parameters of crystals used in rotating-drum spectrometer (RDS) and corresponding spectral ranges: "front" and "rear" refer to wavelength bands covered by front and rear pairs of detectors.

No.	Crystal	Orientation	2d [Å]	Spectral range (front) [Å]	Spectral range (rear) [Å]	Spectral resolution [mÅ]
1	Si	400	2.715	1.678–2.330	0.442–1.618	0.1
2	Si	220	3.840	2.375–3.295	0.625–2.288	0.2
3, 4	Si	111	6.271	3.878–5.381	1.021–3.737	0.3
5	Quartz	10–11	6.684	4.133–5.735	1.088–3.983	0.3
6	Quartz	10–10	8.514	5.265–7.306	1.386–5.073	0.4
7	ADP	101	10.648	6.585–9.137	1.734–6.345	0.5
8	KAP	001	26.640	16.474–22.859	4.337–15.875	1.3

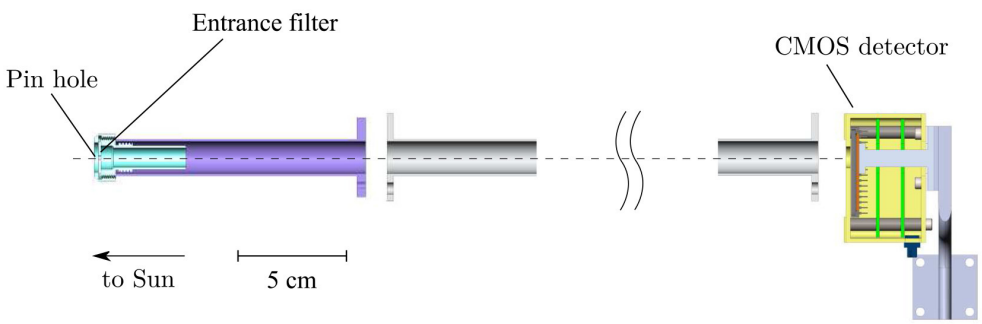

FIGURE 6 | A cross sectional view of the Pin-Hole Imager (PHI) inside the KORTES-SU assembly. The solar disk is projected onto a CMOS sensor placed 70 cm behind a 0.7 mm pin hole.

to increase accuracy of the KORTES pointing system. The main technical parameters of the PHI instrument are listed in **Table 6**.

PHI will take frames every 1/8 s (limited by the CMOS read-out time). Using an on-board processing PHI will find actual positions of ARs, their sizes and orientation. The dispersion direction of the RDS crystals is aligned with the CMOS base allowing to deconvolve real spectral shapes from those observed by RDS. Moreover, we expect that most of the time a single photon per pixel will be detected. This will allow to estimate energy of the incoming radiation. The X-ray intensity averaged over the CMOS area will be used to determine the state of the X-ray corona. The distribution of the emission will help to classify the momentary solar activity into one of three classes: The quiet Sun, the flaring and non-flaring ARs. This information will then be passed to other KORTES instruments in order to switch the mode of observations (e.g., to change exposure time and cadence of telescopes).

7. BRAGG X-RAY SPECTROMETER–POLARIMETER

The Bragg X-ray spectrometer–POLarimeter (B-POL) is a candidate device to be mounted in the KORTES; its deployment is currently under discussion. The optical layout includes a cylindrically bent silicon mono-crystal and a CMOS sensor (see **Figure 7**). The selected spectral range (3.9–4.1 Å) will cover a number of strong emission lines of Ar XVI, Ar XVII, and S XVI, which are nearly always emitted by the coronal sources activity above GOES B5.0 class level. The utilized 2k×2k GSENSE400 BSI CMOS sensor will provide an exceptional spectral resolution of $\sim$ 90 μÅ/bin. The main technical parameters of the B-POL instrument are listed in **Table 7**.

It appears that for the selected [111] orientation of silicon with $2d \approx 6.3$ Å the Bragg angle for the given spectral range is close to Brewster angle ($\sim$ 45°). It means that for a linearly

TABLE 6 | Main characteristics of pin-hole X-ray imager (PHI).

Spectral range	E > 0.35 keV
Entrance filter	Aluminized polyimide foil (15 μm)
Pin hole diameter	0.7 mm
Projection distance	703 mm
Detector type	CMOS (Gpixel GSENSE400, BSI)
Detector size	2048×2048
Pixel size	11 μ
Field of view	1.8°
Frame rate	∼10 fps
Exposure time	0.02–0.1 s

TABLE 7 | Main characteristics of Bragg X-ray spectrometer-polarimeter (B-POL).

Spectral range	3.9–4.1 Å
Target ions (lines)	Ar XVII (w, x, y, z), S XV (w4)
Entrance filter	Aluminized polyimide foil (11 μm)
Mirrors	Bent silicon (cylindrical), [111] lattice plane, $2d \approx 6.3$ Å
Curvature radius	820.97 mm
Spectral resolution	90 μÅ per bin
Detector type	CMOS (Gpixel GSENSE400, BSI)
Detector size	2,048×2,048
Pixel size	11 μ
Pointing range (accuracy)	±1° (1′)

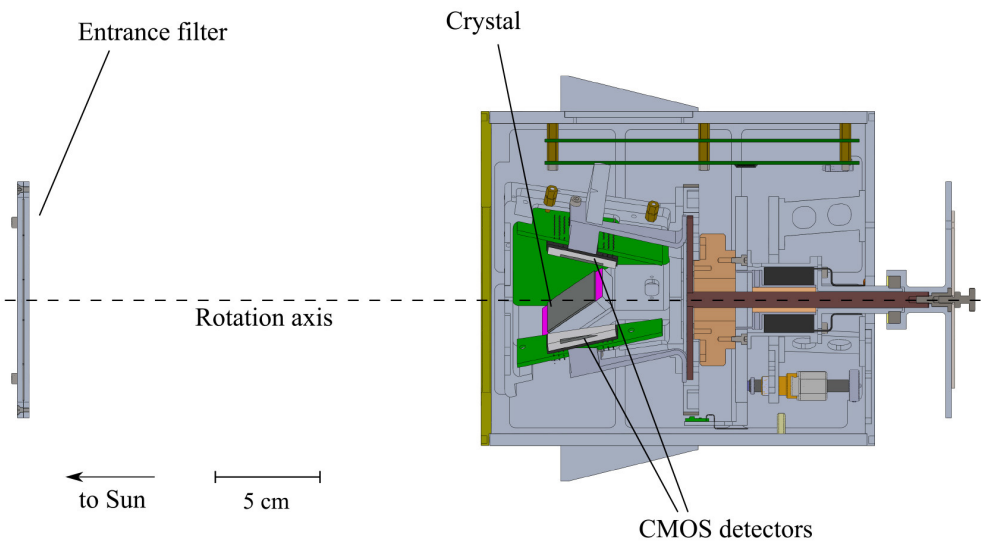

FIGURE 7 | A cross sectional view of the Bragg X-ray spectrometer–polarimeter (B-POL) inside the KORTES-SU assembly. The table with two silicon crystals (mounted at Brewster angle) and two CMOS sensors is spinning around an axis pointing to a solar X-ray source at 1 turn per second.

polarized radiation the reflection efficiency will strongly depend on the orientation of the polarization vector with respect to the plane of incidence (it is maximized for s-polarization). In order to estimate the direction and the degree of polarization B-POL will continuously spin around its optical axis and measure the resulting modulation of the signal.

The rotation rate is selected at 1 turn per second—a compromise between the CMOS readout time and the expected rate of polarization fluctuations. The pointing of the rotation axis will be realized by inclining the support of the rotation table to the desired direction within an angular range of $\pm 1^{\circ}$ with an accuracy better than $1'$. The selection of the source will be based on the readings of PHI. To account for possible misalignment of the rotation axis with the direction to the source B-POL will consist of two identical crystal-detector sections mounted symmetrically on the rotation table. Such a position will also allow to estimate possible Doppler shifts of the X-ray lines to supplement observations from RDS.

B-POL is to be placed in the rear section on KORTES-SU in order to keep the rotating radiator (fixed to the rotating table) in constant shadow. This should allow to cool the polarimeter's CMOS sensors down to -20°C.

8. ATTITUDE CONTROL SYSTEM

The attitude control system of KORTES consists of two Sun sensors (the primary and the backup) and a star tracker. These devices are custom-made by XRAS. The Sun sensors are used to feed the APS systems of KORTES instruments and represent ordinary pinhole cameras. The displacement of the Sun image projected by a pin hole is calculated via the readings of the quadrant Si-pin photodiode (Hamamatsu S5981).

The star tracker is used to control the orientation of KORTES-SU. It is placed in the rear chamber of the unit and is directed orthogonally to its main axis. It consists of a lens, a 1 ×1 k BSI CCD-sensor (e2v 47-20) and a 130 mm-long baffle to shade from the Sun. The tracker has relatively narrow FoV ($\sim$ 15°) to avoid possible flares from the nearest ISS structures. The lens aperture amounts to 25 mm to enable the detection of stars with a magnitude up to $\sim$ 7. The star catalog loaded in the KORTES-EU memory will allow an on-board star identification and attitude determination (Shuster, 2006; Fan and Zhong, 2018). The main parameters of the KORTES attitude control system are listed in **Table 8**.

TABLE 8 | Main characteristics of attitude control system.

Sun sensor	
Pin hole diameter	3 mm
Projection distance	115 mm
Detector type	Quadrant Si-pin photodiode (Hamamatsu S5981)
Detector size	10×10 mm
Update rate	100 Hz
Attitude determination accuracy	$\sim 0.1''$
Star tracker	
Aperture diameter	25 mm
Focal length	50
Detector type	CCD (e2v 47-20, BSI, frame transfer)
Detector size	1024×1024
Pixel size	13 μm
Field of view	$\sim 15^{\circ}$
Baffle rejection angle	$\sim 40^{\circ}$
Frame rate	1–10 fps
Typical exposure time	0.1–1 s
Maximum star magnitude	7
Attitude determination accuracy	$\sim 1'$ (pitch, yaw), $\sim 7'$ (roll)

9. ELECTRONICS UNIT

The KORTES-EU unit represents a small electronics box placed inside the sealed compartment of the ISS Russian segment and is used to gather, store, pre-process, and transfer data incoming from KORTES-SU. KORTES-EU consists of a single electronics board with a number of connectors and a cooling fan. The core operations of KORTES-EU are executed on ACTEL A3PE1500 FPGA with ARM Cortex-M1 soft processor support. KORTES-EU receives data from the KORTES-SU sensors via the Hotlink interface and sends it to the ISS board computer via the Ethernet connection. The data transferring is organized by means of a simple client-server logic based on the NFSv4 protocol. The same data channel is used to update the internal firmware and software of the KORTES units and to run the dedicated program of observations. Concurrently, KORTES-EU saves all incoming data on a USB flash drive. The ISS crew members will be requested to swap the drive when it runs out of free storage. Though the operation of KORTES-EU is stand-alone, the remote serial port access is also supported (in case of emergency).

SUMMARY

The KORTES assembly is the first solar oriented mission for the ISS Russian segment. Though the deployment on board ISS introduces significant challenges regarding pointing and stabilization issues, it has several advantages with respect to restrictions on mass, sizes and telemetry rate. The scientific instrumentation of KORTES consists of several imagers and spectrometers providing the multi-channel observations of the solar atmosphere, crucial for solar activity monitoring. The KORTES full-Sun EUV telescopes and spectroheliographs will provide important data for plasma diagnostics during solar flares, CMEs, and eruptions. The X-ray imagers and spectrometers will measure fluxes, Dopper shifts, and polarization of emission both in lines and continuum. These measurements will make significant contribution to understanding of how magnetic energy is released and dissipated in the solar corona.

The project development is now proceeding to the stage of certification and qualification. The launch of KORTES is

scheduled on 2024. The declared time of on-orbit operation is 3 years. The level-1 data products (images and spectra) will be provided to researchers within inter-institutional agreement right after the launch.

DATA AVAILABILITY STATEMENT

The original contributions presented in the study are included in the article/supplementary material, further inquiries can be directed to the corresponding author/s.

AUTHOR CONTRIBUTIONS

All authors listed have made a substantial, direct and intellectual contribution to the work, and approved it for publication.

FUNDING

The research was funded by Lebedev Physical Institute of the Russian Academy of Sciences.

REFERENCES

Akhsakhalyan, A. A., Akhsakhalyan, A. D., Garakhin, S. A., Erkhova, N. F., Kirichenko, A. S., Kuzin, S. V., et al. (2019). Fabrication and study of a concave crystal mirror for the KORTES project. *J. Tech. Phys.* 64, 1680–1683. doi: 10.1134/S1063784219110033

Bogachev, S. A., Chkhalo, N. I., Kuzin, S. V., Pariev, D. E., Polkovnikov, V. N., Salashchenko, N. N., et al. (2016). Advanced materials for multilayer mirrors for extreme ultraviolet solar astronomy. *Appl. Opt.* 55:2126. doi: 10.1364/AO.55.002126

Bogachev, S. A., Ulyanov, A. S., Kirichenko, A. S., Loboda, I. P., and Reva, A. A. (2020). Microflares and nanoflares in the solar corona. *Phys. Uspekhi* 63, 783–800. doi: 10.3367/UFNe.2019.06.038769

Brown, P. (2019). "Challenges and solutions for precision solar pointing on the ISS for the TSIS instrument," in *2019 IEEE Aerospace Conference* (Big Sky, MT) 1–8. doi: 10.1109/AERO.2019.8742206

Brueckner, G. E., Howard, R. A., Koomen, M. J., Korendyke, C. M., Michels, D. J., Moses, J. D., et al. (1995). The large angle spectroscopic coronagraph (LASCO). *Solar Phys.* 162, 357–402. doi: 10.1007/BF00733434

Byrne, J. P., Morgan, H., Seaton, D. B., Bain, H. M., and Habbal, S. R. (2014). Bridging EUV and white-light observations to inspect the initiation phase of a "two-stage" solar eruptive event. *Solar Phys.* 289, 4545–4562. doi: 10.1007/s11207-014-0585-8

Chkhalo, N. I., Kuzin, S. V., Lopatin, A. Y., Luchin, V. I., Salashchenko, N. N., Zuev, S. Y., et al. (2018). Improving the optical and mechanical characteristics of aluminum thin-film filters by adding thin cap layers. *Thin Solid Films* 653, 359–364. doi: 10.1016/j.tsf.2018.03.051

Fan, Q., and Zhong, X. (2018). A triangle voting algorithm based on double feature constraints for star sensors. *Adv. Space Res.* 61, 1132–1142. doi: 10.1016/j.asr.2017.11.042

Garakhin, S. A., Barysheva, M. M., Vishnyakov, E. A., Zuev, S. Y., Kirichenko, A. S., Kuzin, S. V., et al. (2020). Broadband mirrors for spectroheliographs at the KORTES sun study facility. *J. Tech. Phys.* 65, 1792–1799. doi: 10.1134/S1063784220110109

Kirichenko, A. S., and Bogachev, S. A. (2013). Long-duration plasma heating in solar microflares of X-ray class A1.0 and lower. *Astron. Lett.* 39, 797–807. doi: 10.1134/S1063773713110042

Kirichenko, A. S., and Bogachev, S. A. (2017a). Plasma heating in solar microflares: statistics and analysis. *Astrophys. J.* 840:45. doi: 10.3847/1538-4357/aa6c2b

Kirichenko, A. S., and Bogachev, S. A. (2017b). The relation between magnetic fields and x-ray emission for solar microflares and active regions. *Solar Phys.* 292:120. doi: 10.1007/s11207-017-1146-8

Kuzin, S. V., Reva, A. A., Bogachev, S. A., Erkhova, N. F., Salashchenko, N. N., Chkhalo, N. I., et al. (2020). Application of novel multilayer normal-incidence mirrors for EUV solar spectroscopy. *J. Tech. Phys.* 65, 1736–1739. doi: 10.1134/S1063784220110171

Kuzin, S. V., Shestov, S. V., Bogachev, S. A., Pertsov, A. A., Ulyanov, A. S., and Reva, A. A. (2011a). Processing method of images obtained during the TESIS/CORONAS-PHOTON experiment. *Solar Syst. Res.* 45, 174–181. doi: 10.1134/S0038094611020122

Kuzin, S. V., Zhitnik, I. A., Shestov, S. V., Bogachev, S. A., Bugaenko, O. I., Ignat'ev, A. P., et al. (2011b). The TESIS experiment on the CORONAS-PHOTON spacecraft. *Solar Syst. Res.* 45, 162–173. doi: 10.1134/S0038094611020110

Lemen, J. R., Title, A. M., Akin, D. J., Boerner, P. F., Chou, C., Drake, J. F., et al. (2012). The atmospheric imaging assembly (AIA) on the solar dynamics observatory (SDO). *Solar Phys.* 275, 17–40. doi: 10.1007/978-1-4614-3673-7_3

Loboda, I. P., and Bogachev, S. A. (2015a). Quiescent and eruptive prominences at solar minimum: a statistical study via an automated tracking system. *Solar Phys.* 290, 1963–1980. doi: 10.1007/s11207-015-0735-7

Loboda, I. P., and Bogachev, S. A. (2015b). Velocity field and loss of mass in solar macrospicules from high time resolution observations in the He ii 304 Å spectral line. *Phys. Proc.* 74, 328–335. doi: 10.1016/j.phpro.2015.09.251

Loboda, I. P., and Bogachev, S. A. (2017). Plasma dynamics in solar macrospicules from high-cadence extreme-UV observations. *Astron. Astrophys.* 597:A78. doi: 10.1051/0004-6361/201527559

Loboda, I. P., and Bogachev, S. A. (2019). What is a macrospicule? *Astrophys. J.* 871:230. doi: 10.3847/1538-4357/aafa7a

Reva, A., Shestov, S., Bogachev, S., and Kuzin, S. (2012). Investigation of hot X-ray points (HXPs) using spectroheliograph Mg xii experiment data from CORONAS-F/SPIRIT. *Solar Phys.* 276, 97–112. doi: 10.1007/s11207-011-9883-6

Reva, A., Shestov, S., Zimovets, I., Bogachev, S., and Kuzin, S. (2015). Wave-like formation of hot loop arcades. *Solar Phys.* 290, 2909–2921. doi: 10.1007/s11207-015-0769-x

Reva, A., Ulyanov, A., Kirichenko, A., Bogachev, S., and Kuzin, S. (2018). Estimate of the upper limit on hot plasma differential emission measure (DEM) in non-flaring active regions and nanoflare frequency based on the Mg xii spectroheliograph data from CORONAS-F/SPIRIT. *Solar Phys.* 293:140. doi: 10.1007/s11207-018-1363-9

Reva, A. A., Kirichenko, A. S., Ulyanov, A. S., and Kuzin, S. V. (2017). Observations of the coronal mass ejection with a complex acceleration profile. *Astrophys. J.* 851:108. doi: 10.3847/1538-4357/aa9986

Reva, A. A., Ulyanov, A. S., Bogachev, S. A., and Kuzin, S. V. (2014). Initiation and early evolution of the coronal mass ejection on 2009 may 13 from extreme-ultraviolet and white-light observations. *Astrophys. J.* 793:140. doi: 10.1088/0004-637X/793/2/140

Reva, A. A., Ulyanov, A. S., and Kuzin, S. V. (2016a). Current sheet structures observed by the TESIS EUV telescope during a flux rope eruption on the sun. *Astrophys. J.* 832:16. doi: 10.3847/0004-637X/832/1/16

Reva, A. A., Ulyanov, A. S., Shestov, S. V., and Kuzin, S. V. (2016b). Breakout reconnection observed by the TESIS EUV telescope. *Astrophys. J.* 816:90. doi: 10.3847/0004-637X/816/2/90

Rodkin, D., Slemzin, V., Zhukov, A. N., Goryaev, F., Shugay, Y., and Veselovsky, I. (2018). Single ICMEs and complex transient structures in the solar wind in 2010 - 2011. *Solar Phys.* 293:78. doi: 10.1007/s11207-018-1295-4

Schweizer, F. (1979). Anamorphic magnification of grating spectrographs - a reminder. *Pub. Astron. Soc. Pac.* 91:149. doi: 10.1086/130458

Shestov, S., Nakariakov, V. M., and Kuzin, S. (2015). Fast magnetoacoustic wave trains of sausage symmetry in cylindrical waveguides of the solar corona. *Astrophys. J.* 814:135. doi: 10.1088/0004-637X/814/2/135

Shestov, S., Reva, A., and Kuzin, S. (2014). Extreme ultraviolet spectra of solar flares from the extreme ultraviolet spectroheliograph SPIRIT onboard the CORONAS-F satellite. *Astrophys. J.* 780:15. doi: 10.1088/0004-637X/780/1/15

Shestov, S. V., Nakariakov, V. M., Ulyanov, A. S., Reva, A. A., and Kuzin, S. V. (2017). Nonlinear evolution of short-wavelength torsional alfvén waves. *Astrophys. J.* 840:64. doi: 10.3847/1538-4357/aa6c65

Shestov, S. V., Ulyanov, A. S., Vishnyakov, E. A., Pertsov, A. A., and Kuzin, S. V. (2014). "Complex of instrumentation KORTES for the EUV and x-ray imaging and spectroscopy of the solar corona," in *Space Telescopes and Instrumentation 2014: Ultraviolet to Gamma Ray, Vol. 9144 of Proc. SPIE* (Montréal, QC). doi: 10.1117/12.2055946

Shestov, S. V., Urnov, A. M., Kuzin, S. V., Zhitnik, I. A., and Bogachev, S. A. (2009). Electron density diagnostics for various plasma structures of the solar corona based on Fe XI-FeXIII lines in the range 176 207 Å measured in the SPIRIT/CORONAS-F experiment. *Astron. Lett*. 35, 45–56. doi: 10.1134/S106377370901006X

Shugay, Y., Slemzin, V., Rodkin, D., Yermolaev, Y., and Veselovsky, I. (2018). Influence of coronal mass ejections on parameters of high-speed solar wind: a case study. *J. Space Weath. Space Clim*. 8:A28. doi: 10.1051/swsc/2018015

Shuster, M. D. (2006). The quest for better attitudes. *J. Astron. Sci*. 54, 657–683. doi: 10.1007/BF03256511

Slemzin, V., Ulyanov, A., Gaikovich, K., Kuzin, S., Pertsov, A., Berghmans, D., et al. (2016). Validation of Earth atmosphere models using solar EUV observations from the CORONAS and PROBA2 satellites in occultation mode. *J. Space Weath. Space Clim*. 6:A7. doi: 10.1051/swsc/2015045

Slemzin, V. A., Goryaev, F. F., Rodkin, D. G., Shugay, Y. S., and Kuzin, S. V. (2019). Formation of coronal mass ejections in the solar corona and propagation of the resulting plasma streams in the heliosphere. *Plasma Phys. Rep*. 45, 889–920. doi: 10.1134/S1063780X19100076

Stęślicki, M., Sylwester, J., Płocieniak, S., Bakała, J., Szaforz, Ż., Ścisłowski, D., et al. (2016). "Soft X-ray polarimeter-spectrometer SOLPEX," in *Solar and Stellar Flares and Their Effects on Planets, Vol. 320*, eds A. G. Kosovichev, S. L. Hawley, and P. Heinzel (Honolulu, HI: Cambridge University Press), 450–455. doi: 10.1017/S1743921316002106

Sylwester, B., Faucher, P., Jakimiec, J., Krutov, V. V., and McWhirter, R. W. P. (1986). Investigation of the MG XII 8.42 A doublet in solar flare spectra. *Solar Phys*. 103, 67–87. doi: 10.1007/BF00154859

Sylwester, J., Stęślicki, M., Bąkała, J., Płocieniak, S., Szaforz, Ż., Kowaliński, M., et al. (2019). The soft X-ray spectrometer polarimeter SolpeX. *Exp. Astron*. 47, 199–223. doi: 10.1007/s10686-018-09618-4

Ulyanov, A. S., Bogachev, S. A., and Kuzin, S. V. (2010). Bright points and ejections observed on the sun by the KORONAS-FOTON instrument TESIS. *Astron. Rep*. 54, 948–957. doi: 10.1134/S1063772910100082

Ulyanov, A. S., Bogachev, S. A., Loboda, I. P., Reva, A. A., and Kirichenko, A. S. (2019a). Direct evidence for magnetic reconnection in a solar EUV nanoflare. *Solar Phys*. 294:128. doi: 10.1007/s11207-019-1472-0

Ulyanov, A. S., Bogachev, S. A., Reva, A. A., Kirichenko, A. S., and Loboda, I. P. (2019b). The energy distribution of nanoflares at the minimum and rising phase of solar cycle 24. *Astron. Lett*. 45, 248–257. doi: 10.1134/S1063773719040078

Vishnyakov, E. A., Bogachev, S. A., Kirichenko, A. S., Reva, A. A., Loboda, I. P., Malyshev, I. V., et al. (2017). "Joint observations of solar corona in space projects ARKA and KORTES," in *EUV and X-RAY Optics: Synergy Between Laboratory and Space V, Vol. 10235 of Proceedings of SPIE, SPIE-INT SOC Optical Engineering, Conference on EUV and X-ray Optics - Synergy Between Laboratory and Space V*, eds R. Hudec and L. Pina (Prague). doi: 10.1117/12.2264989

Vishnyakov, E. A., Kirichenko, A. S., Reva, A. A., Rizvanov, A. A., Plastinin, J. A., and Kuzin, S. V. (2016). "Spectral calibration of CCDs and multilayer filters intended for future space applications," in *Space Telescopes and Instrumentation 2016: Ultraviolet to Gamma Ray, Vol. 9905 of Society of Photo-Optical Instrumentation Engineers (SPIE) Conference Series*, eds J. W. A. den Herder, T. Takahashi, and M. Bautz, (Edinburgh). doi: 10.1117/12.2231410

Zhang, J., Dere, K. P., Howard, R. A., Kundu, M. R., and White, S. M. (2001). On the temporal relationship between coronal mass ejections and flares. *Astrophys. J*. 559, 452–462. doi: 10.1086/322405

Zhitnik, I. A., Bougaenko, O. I., Delaboudiniere, J.-P., Ignatiev, A. P., Korneev, V. V., Krutov, V. V., et al. (2002). "SPIRIT X-ray telescope/spectroheliometer results," in *Solar Variability: From Core to Outer Frontiers, Vol. SP-506 of ESA*, ed A. Wilson (Noordwijk), 915–918.

Zhitnik, I. A., Bugaenko, O. I., Ignat'ev, A. P., Krutov, V. V., Kuzin, S. V., Mitrofanov, A. V., et al. (2003). Dynamic 10 MK plasma structures observed in monochromatic full-Sun images by the SPIRIT spectroheliograph on the CORONAS-F mission. *Mon. Not. Roy. Astron. Soc*. 338, 67–71. doi: 10.1046/j.1365-8711.2003.06014.x

Conflict of Interest: The authors declare that the research was conducted in the absence of any commercial or financial relationships that could be construed as a potential conflict of interest.